PERGAMON

Journal of Structural Geology 22 (2000) 1663–1674

JOURNAL OF STRUCTURAL GEOLOGY

www.elsevier.nl/locate/jstrugeo

Albite crystallographic preferred orientation and grain misorientation distribution in a low-grade mylonite: implications for granular flow

Zhenting Jiang*, David J. Prior, John Wheeler

Jane Herdman Laboratories, Department of Earth Sciences, University of Liverpool, Liverpool L69 3GP, UK

Received 12 December 1999; accepted 8 June 2000

Abstract

Crystallographic orientation data from pure albite domains in a low-grade sheared metagabbro from the Combin Zone of the western Italian Alps were measured by electron backscatter diffraction. Crystallographic preferred orientations (CPOs) in four high-strain domains are non-random and have a triclinic symmetry. The clusters of [100], [010] and [001] show an angular relationship that corresponds to that of the albite crystal lattice. However, the orientations of axis clusters to the kinematic axes vary from domain to domain. CPOs from a low-strain domain also show clustered axes with triclinic symmetry, but with more intense clustering than those in the high-strain domains. Grain misorientation distributions are presented both for the low-strain domain and one of the high-strain domains. In the high-strain domain, the distribution of misorientation angles between neighbouring grains displays a peak at about 70°. The equivalent distribution in the low-strain domain has a peak at 30°. For both domains, the misorientation axis distributions, between neighbouring and non-neighbouring grains, are random, except for some of axes with 160–180° misorientation that exhibit a slight concentration around [010]. The diversity of CPOs among the domains suggests that these CPOs could not be produced by dislocation creep. They are likely to have been inherited from plagioclase parents, as a result of host control on the nucleation of the new albite grains. These CPOs do not contain any direct information about the deformation kinematics. We interpret that deformation of these domains occurred by granular flow. Crystallographic axis dispersion due to grain boundary sliding (GBS) caused weakening of CPOs, modification of misorientation angle distributions and randomisation of misorientation axis distributions. The fact that a CPO can survive GBS even after a high strain indicates that CPO is not always a sensitive indicator of deformation mechanisms. Misorientation distribution may provide a complementary, and possibly a more sensitive indicator of deformation mechanisms. Published by Elsevier Science Ltd.

1. Introduction

Crystallographic preferred orientations (CPOs) of shear zone rocks contain important information about deformation kinematics in terms of strain, strain symmetry and deformation mechanisms (e.g. Schmid and Casey, 1986). CPOs are used to constrain active slip systems, where rocks have deformed by intracrystalline plasticity (op cit.). Unfortunately, CPOs from naturally deformed rocks cannot, in many cases, be interpreted unambiguously. The reason is our lack of understanding of the physical processes of texture formation (Wenk and Christie, 1991). Numerical modelling has proven to be a useful tool (Lister et al., 1978; Jessell, 1988; Wenk et al., 1989; Casey and McGrew, 1999), and studying CPO in experimentally and naturally deformed samples is an important approach to a better understanding of texture-forming processes (e.g. Gleason et al., 1993). However, the approach of measuring only the bulk CPO neglects crucial information about intragrain and intergrain processes in CPO formation. Electron backscatter diffraction (EBSD) in scanning electron microscopy (SEM) enables measurement of the complete crystallographic orientation of individual grains for grain sizes down to 1 μm (Prior et al., 1999). Crystallographic data obtained in this way can be used to characterise grain boundaries in terms of their crystallographic misorientation (Lloyd et al., 1987; Randle, 1992, 1993; Lloyd et al., 1997; Trimby et al., 1998). Knowledge of grain boundary misorientations may help us to understand texture-forming processes and deformation mechanisms (Fliervoet et al., 1997; Fliervoet et al., 1999; Leiss and Barber, 1999).

Prior and Wheeler (1999) measured a CPO from a high-stain, fine-grained pure albite domain in a greenschist facies albite-rich mylonite. The CPO displayed triclinic symmetry, and as such could not be easily related to the symmetry of deformation. Prior and Wheeler (1999) suggested two explanations that raised

* Corresponding author.
E-mail address: zjiang@liverpool.ac.uk (Z. Jiang).

0191-8141/00/$ - see front matter. Published by Elsevier Science Ltd.
PII: S0191-8141(00)00079-1

important questions on CPO-forming mechanisms and the deformation mechanisms of albite at low grades:

1. the CPO and its symmetry relate to dislocation creep within a complex strain path, giving rise to a triclinic fabric. This explanation requires albite to deform by dislocation creep in the greenschist facies. There is no evidence that this is possible.
2. the CPO was inherited from a single crystal host, with grain-boundary sliding causing dispersion from the host orientation.

Prior and Wheeler (1999) suggest that analysis of a large portion of the same sample will distinguish these two possibilities. Consistent CPO across large parts of the sample would support the first hypothesis, while inconsistent CPOs in different parts of the sample would support the second hypothesis. In this paper, we conduct this test using a second thin section from the same sample studied by Prior and Wheeler (1999). In addition, we make a more thorough interpretation of deformation and CPO forming mechanisms, based upon crystallographic orientation and misorientation data obtained using SEM-based crystallographic techniques.

2. Sample description

The studied sample 80207 (field 1–24) is a mylonite derived from a metagabbro protolith. It was collected from the Combin Zone of the Western Italian Alps, a kilometre-scale greenschist facies shear zone which unroofed the Piemonte eclogites (Wheeler and Butler, 1993; Reddy et al., 1999). In hand specimen, compositional bands with different colours are found to form an interconnected network surrounding dark green–brown fragments of hornblende and augite with grain size varying from 1 to 6 mm. In three dimensions, these bands define a main mylonitic foliation with an average orientation about 016 18°E, on which a stretching lineation plunging 08° towards 093 is developed. Angular-shaped fragments of hornblende generally have asymmetric tails. These asymmetric structures suggest a non-coaxial strain in the shear zone. On the thin section scale, the sample shows a very inhomogeneous optical microstructure consisting of fractured and broken hornblende porphyroclasts in a fine-grained matrix (Fig. 1). The matrix is composed of albite, zoisite and tremolite with rare chlorite. Two kinds of compositional domain are well developed in the matrix. Pure albite domains (the white bands in hand specimen) consist of fine-grained albite, with less than 1% zoisite. Polymineralic domains are composed of a mixture of fine-grained zoisite, tremolite and albite. A narrow transition zone, characterised by a mixture of fine-grained albite and zoisite, is commonly developed between these two kinds of domain.

The albite is pure An_0 with Ca below the detectable limit of electron microprobe analyses. Zoisite is slightly epidotic with up to 15% Fe/(Fe + Al). According to Stünitz (1993), who carried out a detailed microstructural and geochemical study on a sheared gabbro sample located just 1 km away from our sample, both albite and zoisite are derived from intermediate plagioclase due to retrograde fluid–rock reaction. Tremolite is sodic, but more aluminous with proximity to the hornblende porphyroclasts. Optical observation suggests that albite–zoisite–tremolite–chlorite was the stable assemblage during deformation, giving a greenschist facies P–T condition (temperature 300–450°C and pressure less than 900 MPa).

3. EBSD and OC-imaging techniques

The analytical work was carried out on a Philips XL 30 SEM at 20 kV, with a beam current of about 3 nA, a working distance of about 23 mm and specimen tilt of 70°. Orientation contrast (OC) imaging used two solid-state forescatter detectors (Prior et al., 1996). The OC images provided maps of where crystallographic orientations change. EBSD (Venables and Harland, 1972; Dingley, 1984; Wilkinson and Hirsch, 1997; Prior et al., 1999) was used to measure the crystallographic orientation. EBSD patterns were imaged on a phosphor screen, viewed by a low light SIT camera and indexed using the software package CHANNEL+ (Schmidt and Olesen, 1989). The albite structure-file, used for indexing, was developed by Prior and Wheeler (1999) and contains 96 reflectors. For each indexed grain, a simulated pattern was compared manually to the EBSD pattern to ensure that computer indexing had calculated the correct orientation. The spatial and angular resolutions of this technique are about 1 μm and 1°, respectively.

The thin section was polished using diamond paste on a paper lap followed by chemical–mechanical polishing using SYTON fluid (Lloyd et al., 1987). The sample was not carbon-coated since this significantly reduces the quality of EBSD patterns and OC images. The whole specimen surface, except for the pure albite domains to be measured, was painted with carbon-paint to minimise charging. By switching off the beam after each EBSD measurement, a working time for at least 500 measurements was available before charging prevented analysis.

4. Domainal CPO

To compare the CPO pattern among different domains, four high-strain pure albite domains (labelled A, B, C and D in Fig. 1) were analysed (Domain E, a low-strain domain, will be discussed later). The selected high-strain domains have the following characteristics in common.

1. *High strain*. (a) Domain boundaries are straight and parallel to the main mylonitic foliation, (b) the length

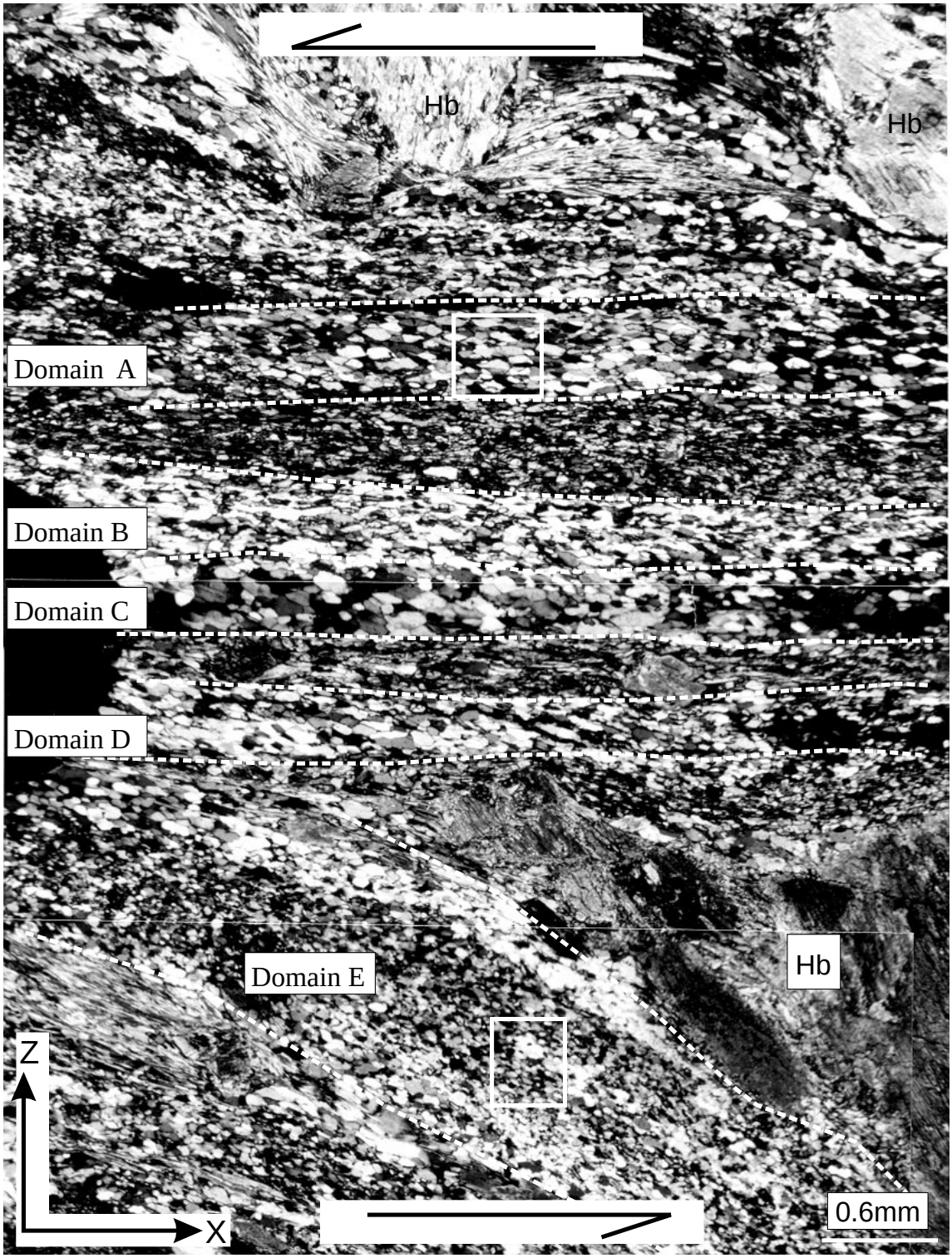

Fig. 1. Optical microstructure of the albite-rich mylonite, showing well-developed compositional domains. Crystallographic orientation data were collected from four high-strain pure albite domains (Domain A, B, C and D) and one low-strain pure albite domain (Domain E) by indexing EBSD patterns. Other parts of the section are polymineralic domains, comprising zoisite, albite, tremolite and hornblende (Hb) clasts. The squares mark the areas from which forescatter OC images in Fig. 3 were taken.

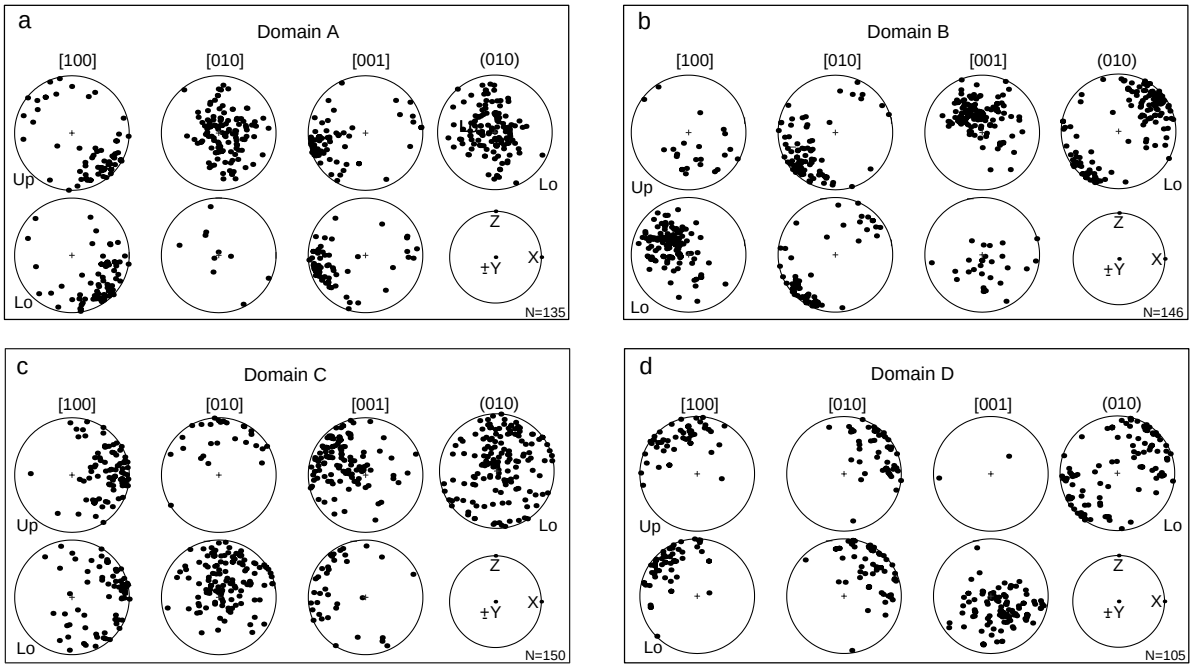

Fig. 2. Domainal CPOs from the high-strain pure albite domains A, B, C and D (Fig. 1). Crystallographic directions ([100], [010], [001]) are plotted on the entire sphere. Up = upper hemisphere, Lo = lower hemisphere. Poles to planes (010)) are plotted on the lower hemisphere. All figures are equal area. The figure in the bottom right of each box shows the plot of the kinematic axes *X*, *Y* and *Z*, with (−Y) inferring the plot on the upper hemisphere and (+*Y*) inferring the plot on the lower hemisphere. *X* is parallel to the lineation. *Z* is the pole to foliation.

to width ratios of domains are greater than 10:1, and (c) albite grains within each domain are elongated with aspect ratios up to about 5:1, although not necessarily with long axes parallel to domain boundaries.

2. *Similar kinematic conditions*. The domains are, in close proximity, enclosed within a width of about 2 mm in the same thin section. This suggests that all domains were deformed under similar kinematic conditions even though they could have enjoyed different strains due to strain heterogeneity at microscopic scale.
3. *Different parents*. Domain A and Domain D are spatially separated from Domain B and Domain C by polymineralic domains of fine-grained zoisite, albite and tremolite (Fig. 1). It is, therefore, expected that these domains were derived from different parent plagioclase clasts. Although Domain B and Domain C are directly adjacent, they are quite different in grain size and shape and therefore can be treated as two different domains. If the albite deformed by dislocation creep, it is expected that CPO patterns from each domain should be comparable, even though CPO intensity may vary as a result of variations in strain magnitude among the domains. It is also expected that the symmetry of the pattern should be coincident with the symmetry of the kinematic framework (Paterson and Weiss, 1961).

To obtain bulk CPOs from each domain, data were collected on a grid, irrespective of imaged grain boundaries. The spacing of grid measurement was chosen to be just above the grain size so that a large data set could be collected, whilst duplicate analyses of single grains were avoided. Depending on the grain size of individual domains, the grid spacing ranged between 50 and 100 μm. Generally, up to about 150 grains from an area about 4–6 mm^2 were measured in each domain. Since albite has triclinic symmetry, both lower and upper hemispheres are required to present the CPO. Orientation patterns of the principal crystallographic axes ([100], [010] and [001]) in all four domains are shown in Fig. 2. Features common to these CPOs and the CPO from a nearby thin section of the same sample as shown by Prior and Wheeler (1999), are summarised as follows.

1. Non-random CPOs are obtained from all four domains. The pole figures of all three principal crystallographic axes are characterised by clusters. There is a slight variation in the intensity of the CPO between the different domains.
2. The CPOs from each domain show triclinic symmetry. The maxima of pole figures for [100], [010] and [001] show angular relationships which are close to those of albite crystal lattice and can therefore be described by α, β and γ, respectively. This may indicate that the triclinic symmetry of pole patterns express not the symmetry of strain, but the symmetry of a parent crystal of plagioclase.
3. With reference to the kinematic axes (*X*, *Y* and *Z*), the CPOs are different from domain to domain. There is no unique orientation relationship between the CPOs and the kinematic axes, which would be expected if the

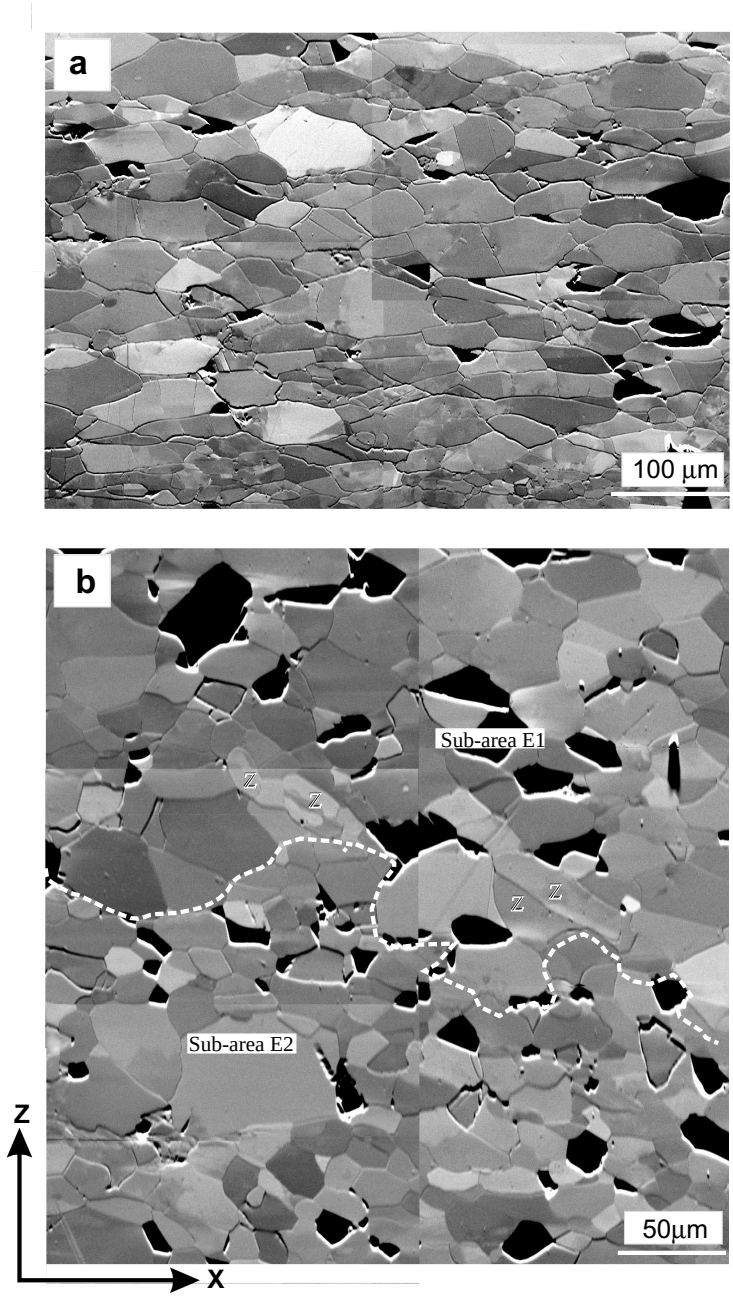

Fig. 3. OC images taken from marked areas in Fig. 1. (a) High-strain Domain A; (b) low-strain Domain E. The broken white line divides (b) into two sub-areas (Sub-area E1 and Sub-area E2) with different grain structure. Z = Zoisite.

CPOs resulted from dislocation creep acting on random initial aggregates under similar kinematic conditions. The diversity in the CPO among different domains probably reflects the diversity of crystallographic orientation of parent plagioclase grains in the gabbro protolith. The orientation patterns of (010), the most common slip plane for plagioclase (Marshall and Mclaren, 1977; Olsen and Kohlstedt, 1984; Ji and Mainprice, 1988; Dornbusch, 1995; Kruse and Stünitz, 1999), also vary between domains. No domain shows a concentration of poles to (010) planes around the pole to the foliation, as is commonly obtained for plagioclase feldspar (Ji and Mainprice, 1988; Dornbusch, 1995; Ji et al., 1988) deformed by dislocation creep.

5. Grain misorientation distribution

The crystallographic misorientation between two crystals

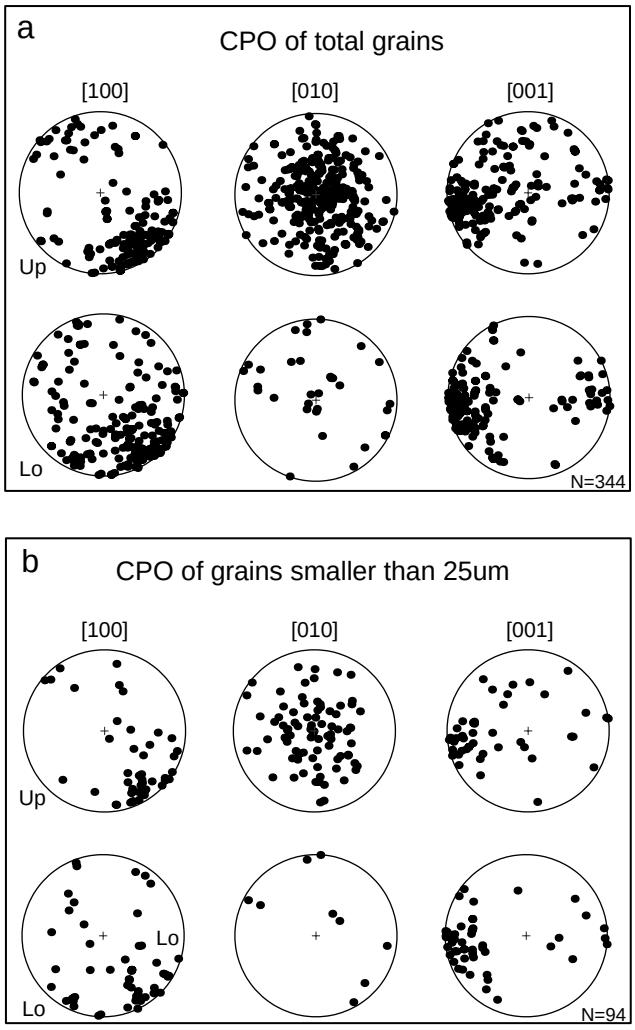

Fig. 4. (a) CPO of all grains in Fig. 3a. (b) CPO of grains with grain size smaller than 25 μm. Crystallographic directions ([100], [010], [001]) are plotted on the entire sphere. Up = upper hemisphere, Lo = lower hemisphere. All figures are equal area. See Fig. 2 for the kinematic reference frame.

can be described in terms of the misorientation axis and angle, named axis–angle pairs (Randle, 1992, 1993; Lloyd et al. 1997; Fliervoet et al., 1999). The misorientation axis is a crystallographic direction shared by both crystals, around which two crystal lattices can be brought into perfect registry after a rotation. The two choices for the axis (+ve and −ve directions of the same line) are equally valid and by convention we plot the one that projects in the hemisphere chosen for the inverse pole figure (IPF). The rotation angle needed for this operation is defined as the misorientation angle, taken as positive by convention.

There are several ways to present misorientation data (Day, 1993; Randle, 1993; Lloyd et al. 1997). The simplest and most straightforward way is to plot the angle data separately from the axis data. Two kinds of plot are needed. The misorientation angle distribution (MAD) is displayed using a histogram of the frequency of different misorientation angles among the grain pairs. Misorientation axes are plotted in an IPF. The misorientation axis distribution (MXD) is shown in a series of IPFs, where each IPF shows axes corresponding to a given range of misorientation angles (Fliervoet, et al., 1999).

Our database for misorientation analyses is the collection of measurements of crystallographic orientations obtained by EBSD. These data allow us to perform two kinds of misorientation analysis. A correlated misorientation is calculated from two orientation measurements, either side of a boundary between neighbouring grains. An uncorrelated misorientation is calculated from the orientations of grain pairs that are not necessarily in physical contact (Fliervoet et al., 1999). The data set size is, in the case of correlated misorientation distribution, related to the number of measured neighbouring grain pairs. In the case of uncorrelated misorientation distribution, all grains might be taken for pairing. In practice this calculation may take too long, so that a random subset is picked. In this study, 500 grain pairs are picked randomly from the orientation database. It is expected that important information about grain boundaries can be detected by comparing the correlated and uncorrelated misorientation distribution (Wheeler et al., in review). In the following section, we present the results from grain misorientation analyses performed on two pure albite domains, representing higher strain and lower strain, respectively. In this way, it is hoped to gain a better understanding about the evolution of misorientation distributions with increasing strain.

5.1. High-strain domain—Domain A

5.1.1. Microstructure and CPO

Domain A (Fig. 1) is separated from adjacent polymineralic domains by straight boundaries. Optical observation confirms that albite grains have little detectable internal structure, such as undulatory extinction or subgrains. The OC image (Fig. 3a), taken from the marked area in this domain (see Fig. 1), shows that the grain size (long axes) of albite varies from 200 μm to less than 20 μm. Albite grains are strongly elongated parallel to main mylonitic foliation, with aspect ratios up to 5:1. The grains have straight boundaries. Only a few 120° triple junctions are present, indicating a non-equilibrium boundary structure. The local CPO (Fig. 4a) obtained from an area of about 0.5 mm^2 is comparable with the bulk CPO of this domain (Fig. 2a), indicating that the CPO is homogeneous within the domain and that the local misorientation distribution is representative of the whole domain. There is no significant difference between the CPO of all the grains (Fig. 4a) and that of grains with size smaller than 25 μm (Fig. 4b).

5.1.2. Grain misorientation distribution

The correlated MAD is non-random, characterised by a

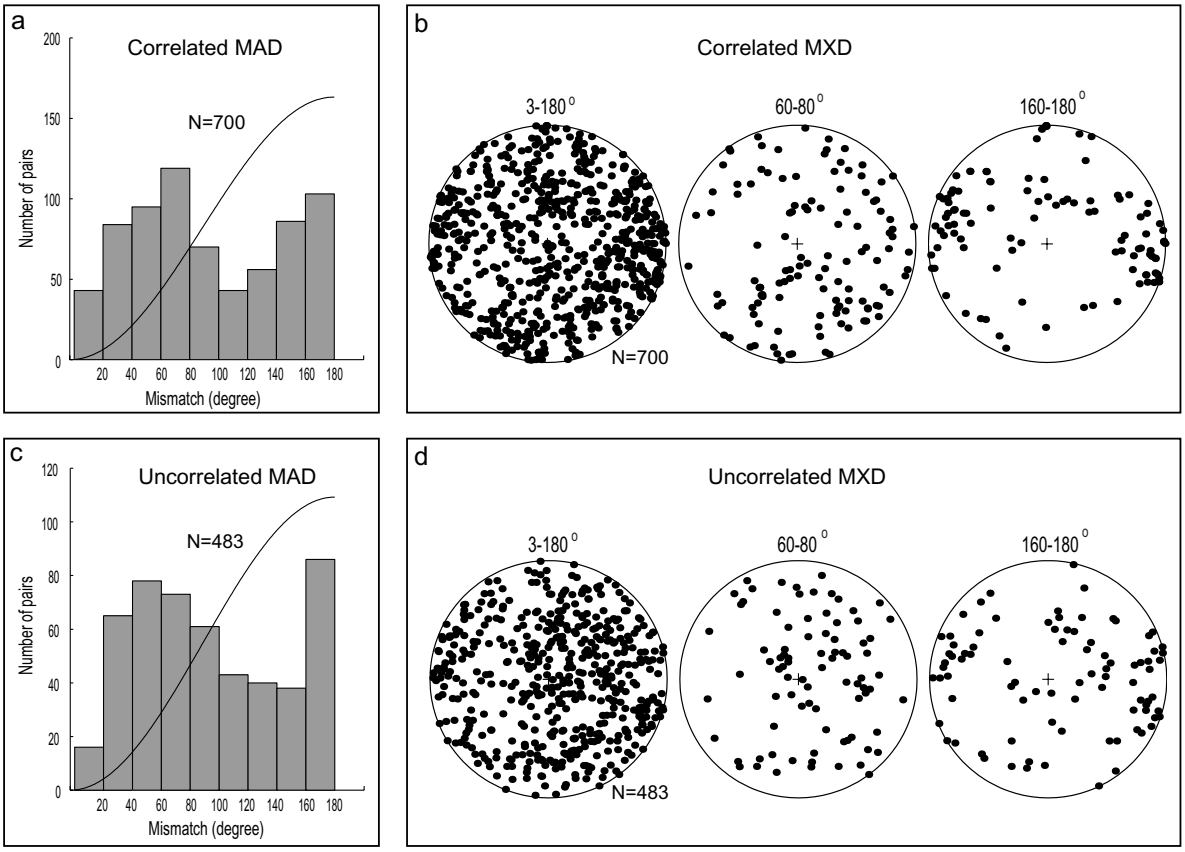

Fig. 5. Grain misorientation distribution of the high-strain domain (Domain A). (a) and (c) are correlated and uncorrelated MADs; (b) and (d) are inverse pole figures showing MXD for correlated and uncorrelated grain pairs, respectively. The thin line in (a) and (c) represents the MAD for a randomly oriented set of triclinic grains (Wheeler et al., in review). Misorientation angles less than 3° have very large axis errors (Prior, 1999) and are excluded from the analysis. See Fig. 8b for the crystallographic reference frame of the IPF.

peak at about 70° and a subpeak at 180° (Fig. 5a). The uncorrelated MAD (Fig. 5c) is very similar to the correlated MAD and statistical comparison of correlated and uncorrelated MADs (Wheeler et al., in review) shows no difference between them. These data suggest that grains are not influenced by their neighbours. The frequency of low angle boundaries (smaller than 20°) is quite low. In contrast to the non-random distribution of misorientation angles, misorientation axes of both correlated and uncorrelated grain pairs are fairly random (Fig. 5b, d). The random distribution is also true for most subgroups of misorientation axes, although misorientation axes with 160–180° misorientation show a slight concentration around [010] (Fig. 5b, d), indicating that some boundaries with 180° misorientation are close, in orientation, to albite-law twin boundaries.

5.2. Low-strain domain—Domain E

5.2.1. Microstructure and CPO

Domain E is located near a large hornblende porphyroclast (Fig. 1) and is evidently protected by this clast from large strain. A low strain in this domain is indicated by the low aspect ratio of the domain. The domain boundaries are controlled by hornblende clasts, oriented at an angle about 40° to the main mylonitic foliation. Fig. 3b is an OC image taken from the marked area in this domain (Fig. 1) and can be divided into two sub-areas according to the microstructure. Sub-area E1 (the upper-right part) is composed of grains with size ranging from 10 to 50 μm, whereas sub-area E2 (the lower-left part) is dominated by grains with uniform grain size of about 20 μm. Albite grains in both sub-areas are characterised by almost equant grain shapes, forming a mosaic with straight grain boundaries and well-developed 120° triple junctions. The OC image also shows that albite grains are free of subgrains.

The CPOs from both sub-areas are non-random and show triclinic symmetry (Fig. 6a, b) as displayed in the CPOs of the high-strain domains (Figs. 2 and 4). However, the CPO patterns from sub-area E1 and sub-area E2 are different, suggesting that albite grains in these sub-areas were also derived from two different parents. The intensity of the CPOs in the low-strain domain is clearly higher than that of CPOs in the high-strain domain (comparing Fig. 6 with Fig. 4).

5.2.2. Grain misorientation distribution

The misorientation distributions from both sub-areas are similar to each other (Fig. 7). The correlated MAD is not

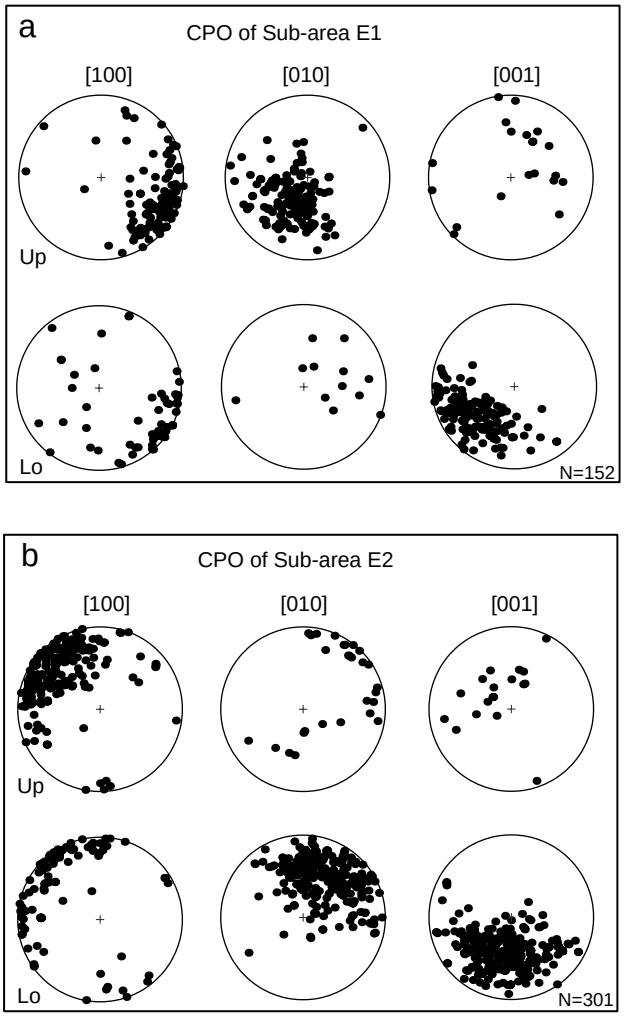

Fig. 6. CPOs from two sub-areas in the low-strain domain (Domain E). Crystallographic directions ([100], [010], [001]) are plotted on the entire sphere. Up = upper hemisphere, Lo = lower hemisphere. All figures are equal area. See Fig. 2 for the kinematic reference frame.

random and shows a sharp peak at 30° (Fig. 7a, e). This peak occurs at lower misorientation angles than the main peak in the MAD of the high-strain domain (Fig. 5a). Boundaries with 160–180° misorientation are not common in the low-strain domain. The uncorrelated MAD (Fig. 7c, g) is very similar to the correlated MAD. Both correlated (Fig. 7b, f) and uncorrelated (Fig. 7d, h) misorientation axis distributions are random across a large range of misorientation angles, with the exception of 160–180° misorientation axes. Some of the 160–180° misorientation axes are clustered near the [010], indicating that many of them are close, in orientation, to albite law (Smith, 1974) twin boundaries. The misorientation distribution of all the grains in Fig. 3b is distinctly different from that of either of the two sub-areas. The uncorrelated MAD of all grains has a major peak at 160° and a subpeak at 50° (Fig. 8a). The subpeak is clearly related to the misorientation relationship inside each sub-area, whereas the major peak reflects the misorientation relationship between the two sub-areas. The strong concentration of axes with 160–180° misorientation around [001] (Fig. 8b) indicates that albite grains in both sub-areas may be derived from two parts of a single Carlsbad twinned (Smith, 1974) plagioclase.

6. Discussion

6.1. Texture and deformation mechanism

There are few published measurements of albite CPOs in the literature and slip systems in albite are not well known. However, it should be reasonable to expect that albite possesses similar slip systems to other plagioclases and albite CPO patterns should be comparable with that of plagioclase for given deformation conditions. Slip on (010) has been identified using transmission electron microscopy to be important in plagioclase in a range of compositions under amphibolite facies to granulite facies conditions (Marshall and Mclaren, 1977; Olsen and Kohlstedt, 1984; Ji and Mainprice, 1988; Dornbusch, 1995; Kruse and Stünitz, 1999). The dominance of this slip system in plagioclase is consistent with the fact that plagioclase shows concentrations of poles to the (010) plane around the pole to the foliation (Ji and Mainprice, 1988; Dornbusch, 1995; Ji et al., in press).

None of the CPOs presented here has a concentration of poles to the (010) plane around the pole to foliation. In fact, the albite CPO patterns are quite different from domain to domain (Fig. 2) and even in two sub-areas of the same domain (Fig. 6). Since all selected domains are neighbouring domains and should therefore have been deformed under similar kinematic and temperature conditions, the diversity of CPO patterns cannot be explained in terms of kinematics and active slip systems. Strain partitioning and strain heterogeneity on the thin section scale, in naturally deformed rocks, may result in a variation of CPO with microstructural location (Garcia Celma, 1982; Goodwin and Williams, 1996; Jiang, 1998). However, in such cases, CPOs from different domains can still be correlated with the bulk kinematic symmetry. It is obvious that none of the CPOs presented here can be correlated to any single bulk kinematic model, including the kinematic model defined by the shear-zone geometry. The most reasonable interpretation for the diversity of CPOs, corresponding to different fabric domains, and their deviation from a consistent orientation, relative to the kinematic framework, is that the CPOs of the pure albite domains were inherited from their parent plagioclase grain. The parent plagioclase grain controlled the nucleation and crystallographic orientation of new albite grains. The diversity in the CPOs reflects the diversity of crystallographic orientations of parent plagioclase grains in the gabbro protolith. This explanation does not rely on whether albite nucleated before (Stünitz, 1993) or during plagioclase deformation, although it does require

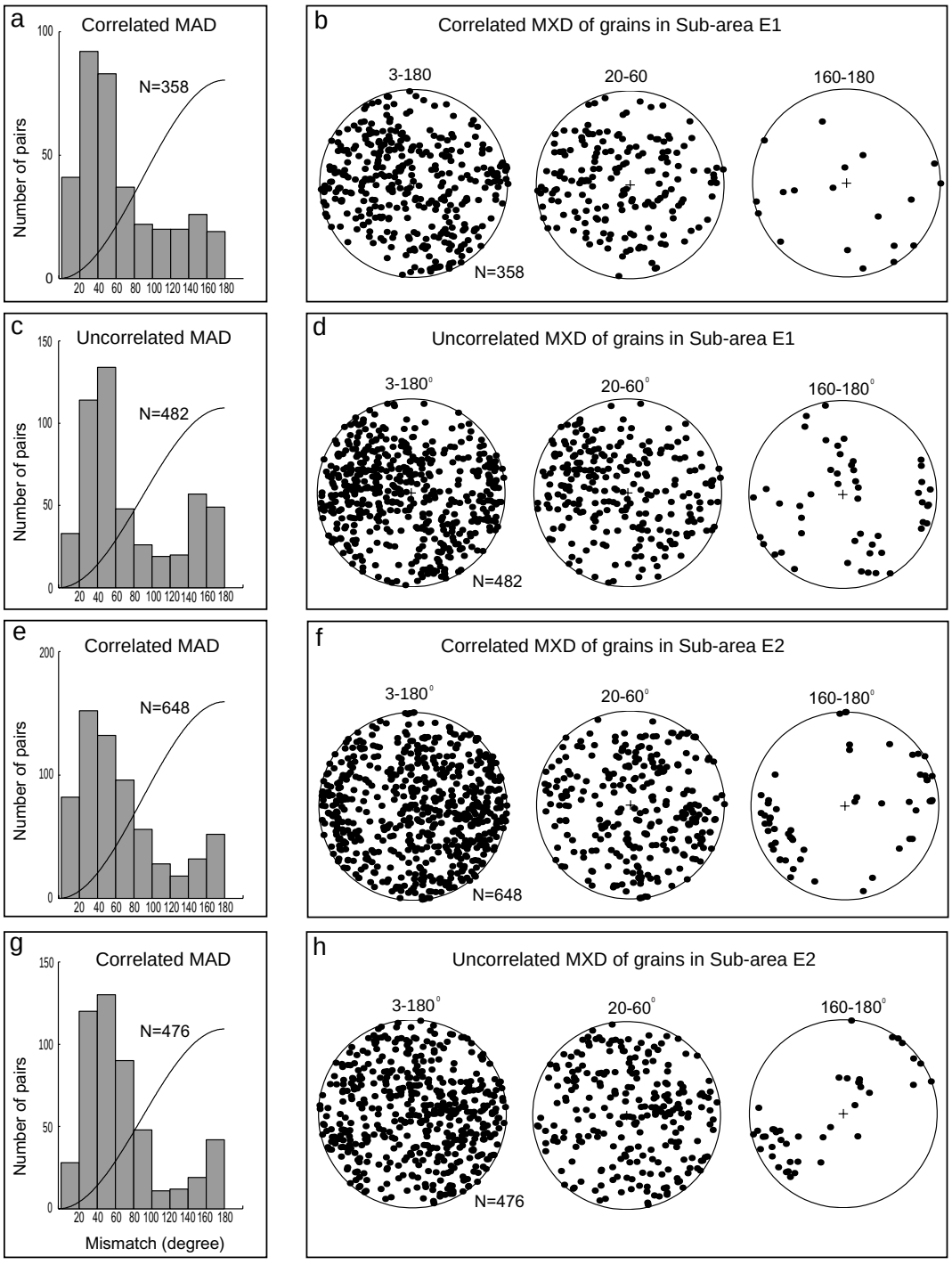

Fig. 7. Grain misorientation distribution of the low-strain domain (Domain E). (a–d) Correlated and uncorrelated MAD and MXD of grains from sub-area E1. The correlated and uncorrelated MAD and MXD of grain in the sub-area E2 are shown in (e–h), respectively. The thin line in (a), (c), (e) and (g) represents the random MAD for triclinic symmetry (Wheeler et al., in review). Misorientation angles less than 3° have very large axis errors (Prior, 1999) and are excluded from the analysis. See Fig. 8b for the crystallographic reference frame of IPF.

that the plagioclase of one domain had little variation in orientation prior to transformation. We have no detailed model as to how exactly albite nucleated and grew, or how pure albite bands were formed. We speculate that the original plagioclase was zoned, so that zoisite nucleated in the Ca-rich parts and may have had difficulty nucleating elsewhere.

There are no published data for grain misorientation distribution of albite in the literature. However, it is useful to compare our albite misorientation distributions with those

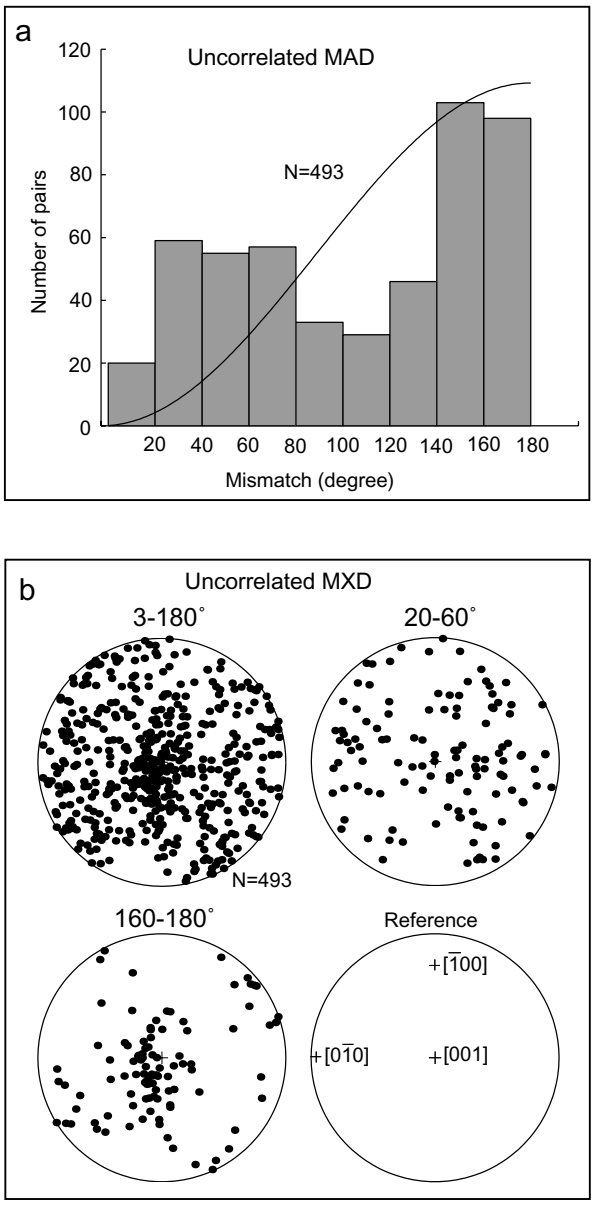

Fig. 8. Uncorrelated MAD (a) and MXD (b) of grains in Fig. 3b. The thin line in (a) represents the random MAD for triclinic symmetry (Wheeler et al., in review). Misorientation angles less than 3° have very large axis errors (Prior, 1999) and are excluded from the analysis. The crystallographic reference frame of IPF for plotting on the upper hemisphere is shown on the bottom right in Fig. 8b.

published for quartz and olivine. Trimby et al. (1998) studied a quartz mylonite deformed by dislocation creep, in the greenschist facies. Trimby (1998) studied a quartzite, deformed experimentally by dislocation creep, in recrystallisation regime III (Hirth and Tullis, 1992). Fliervoet et al. (1999) studied synthetic olivine aggregates deformed by dislocation creep. In all these cases of deformation by dislocation creep, there is a peak (quartz) or subpeak (olivine) in the MAD, corresponding to low misorientation angles (0–20°). Dislocation creep and associated recovery produce a large number of low angle grain boundaries (Trimby et al., 1998). In contrast, olivine deformed experimentally by diffusion creep (Fliervoet et al., 1999) has random MADs and MXDs. The MADs from our pure albite domains are not random, but low angle grain boundaries are uncommon. Not even a subpeak for low angle boundaries is present either in the high-strain domain (Fig. 5) or in the low-strain domain (Fig. 7), suggesting that dislocation creep was not significant.

CPOs and misorientation distributions from albite domains are consistent with inheritance of crystallographic orientations from parent plagioclase clasts in the gabbro protolith, rather than the results of dislocation creep. The CPOs are controlled by the parent crystals and therefore do not contain any direct information about deformation kinematics and active slip systems. In the studied sample, dislocation creep is not a dominant deformation mechanism. Instead, deformation of fine-grained albite aggregates was probably accomplished by a grain size-sensitive process, such as granular flow (a combination of grain boundary sliding and diffusion as defined by Stünitz, 1993).

6.2. Crystal axes dispersion during granular flow

Prior to deformation, individual domains of fine-grained albite should have had a strong CPO, due to parent lattice control on the nucleation of new grains. These initial CPOs will have been modified during subsequent deformation by granular flow. The CPO from the low-strain domain is stronger (Fig. 6) than that from the high-strain domain (Fig. 4), suggesting that there is a texture weakening with increasing strain. Grain boundary sliding (GBS) could result in a progressive dispersion of crystal axes and weakening of the CPO during deformation. This idea is supported by the shift of the peak in the correlated MAD from 30° in the low-strain domain to 70° in the high-strain domain (Figs. 5a and 7a, e). With the exception of axes corresponding to 160–180° misorientations (near twin relationships), MXDs are random in both the low- and high-strain domains. If each domain were originally one plagioclase grain, with some twinning, we would expect most boundaries to have had zero misorientation and an undefined misorientation axis prior to GBS. Even the smallest, random rotations across these boundaries would give rise to a random MXD. Prior to GBS, twins would have had boundary axis–angle pairs defined by the twin law. GBS would cause small, random rotations across these twin boundaries, giving rise to incremental deviations away from the angle–axis pair defined by the twin law.

It is emphasised that GBS has caused dispersion of the CPO, although an initial strong CPO is preserved to high strain. The MAD is modified by GBS. We speculate that the MXD of an aggregate of grains, which have the same initial

orientation, will be randomised very quickly during GBS. Pre-existing high angle boundaries such as twins may be preserved as non-random components in the MXD.

6.3. Grain structure modification during granular flow

The high-strain domain shows a microstructure that is very different from that of the low-strain domain. We find that grain shape and grain size distribution change with increasing strain (see Fig. 3). Since dislocation creep is inferred not to have been the dominant deformation mechanism and GBS by itself does not cause a change in the grain shape, it must be diffusion creep which is responsible for the modification of grain shape. GBS cannot operate in the absence of a boundary transport mechanism unless strongly dilatational. Diffusion creep is often cited as a mechanism that accommodates GBS and allows granular flow. The diffusion can also lead to grain elongation and coarsening although the driving forces for this process are not yet clear in this case.

7. Conclusion

CPOs of pure albite domains in our sample were not produced by dislocation creep. Instead, they were inherited from parent plagioclase grains which control the pattern and symmetry of CPO of albite. Greenschist facies deformation of this fine-grained albite occurred not by dislocation creep, but by granular flow.

GBS is responsible for the dispersion of crystal axes, resulting in a weakening of initially strong CPOs and an increase in the mean misorientation angle of neighbouring grain pairs. Initial strong CPOs can survive, even after high strain by GBS. It is therefore emphasised that the CPO alone may not reflect the deformation mechanisms clearly. Crystallographic misorientation data are an equally relevant, and perhaps more sensitive, indicator of deformation mechanisms.

Acknowledgements

This study is of a part of a research project financially supported by a NERC Grant GR/11768. The reviewers made many valuable comments. In particular, an extremely thorough appraisal by Jan Tullis has enabled us to focus upon and clarify the important points in this paper.

References

Casey, M., McGrew, A.J., 1999. One-dimensional kinematic model of preferred orientation development. Tectonophysics 303, 131–140.

Day, A., 1993. Developments in EBSP technique and their application to grain imaging. Ph.D. thesis, University of Bristol.

Dingley, D.J., 1984. Diffraction from sub-micron area using electron backscattering in a scanning electron microscope. Scanning Electron Microscopy 2, 569–575.

Dornbusch, J., 1995. Gefüge-, Mikrostruktur- und Texturuntersuchungen an Hochtemperatur-Scherzonen in granulitfaziellen Metabasiten der Ivrea-Zone., Geotektonische Forschungen 83.

Fliervoet, T.F., White, S.H., Drury, M.R., 1997. Evidence for dominant grain boundary sliding deformation in greenschist and amphibolite-grade polymineralic mylonites from Redbank deformed zone, Central Australia. Journal of Structural Geology 12, 1495–1520.

Fliervoet, T.F., Drury, M.R., Chopra, P.N., 1999. Crystallographic preferred orientations and misorientations in some olivine rocks deformed by diffusion or dislocation creep. Tectonophysics 303, 1–27.

Garcia Celma, M.A., 1982. Domainal and fabric heterogeneities in the Cap de Creus quartz mylonites. Journal of Structural Geology 4, 433–455.

Gleason, G.C., Tullis, J., Heidelbach, F., 1993. The role of dynamic recrystallization in the development of lattice preferred orientation in experimentally deformed quartz aggregates. Journal of Structural Geology 15, 1145–1168.

Goodwin, L.B, Williams, P.F., 1996. Deformation path partitioning within a transpressive shear zone, Marble Cove, Newfoundland. Journal of Structural Geology 18, 975–990.

Hirth, G., Tullis, J., 1992. Dislocation creep regimes in quartz aggregates. Journal of Structural Geology 14, 145–159.

Jessell, M.W., 1988. Simulation of fabric development in recrystallizing aggregates, I. Description of model. Journal of Structural Geology 10, 771–778.

Ji, S., Mainprice, D., 1988. Natural deformation fabrics of plagioclase: implications for slip systems and seismic anisotropy. Tectonophysics 147, 145–163.

Ji, S., Mainprice, D., Boudier, F., 1988. Sense of shear in high-temperature movement zone from the fabric asymmetry of plagioclase feldspars. Journal of Structural Geology 10, 73–81.

Ji, S., Wirth, R., Rybacki, E., Jiang, Z., in press. High temperature plastic.-deformation of quartz–plagioclase multilayers by layer-normal compression. Journal of Geophysical Research.

Jiang, Z., 1998. Late-Variscan Transpression Tectonics in the Elbe Zone, Saxony (Germany). Cuvillier Verlag, Goettingen.

Kruse, R., Stünitz, H., 1999. Deformation mechanisms and phase distribution in mafic high-temperature mylonites from the Jotun Nappe, southern Norway. Tectonophysics 303, 223–249.

Leiss, B., Barber, D.J., 1999. Mechanisms of dynamic recrystallization in naturally deformed dolomite inferred from EBSP analyses. Tectonophysics 303, 51–69.

Lister, G.S., Paterson, M.S., Hobbs, B.E., 1978. The simulation of fabric development during plastic deformation and its application to quartzite: the model. Tectonophysics 45, 107–158.

Lloyd, G.E., Ferguson, C.C., Law, R.D., 1987. Discriminatory petrofabric analysis of quartz rocks using SEM electron channelling. Tectonophysics 135, 243–249.

Lloyd, G.E., Farmer, A.B., Mainprice, D., 1997. Misorientation analysis and the formation and orientation of subgrain and grain boundaries. Tectonophysics 279, 55–78.

Marshall, D.B., Mclaren, A.C., 1977. The direct observation and analysis of dislocations in experimentally deformed plagioclase feldspars. Journal of Material Science 12, 893–930.

Olsen, T.S., Kohlstedt, D.L., 1984. Analysis of dislocations in some naturally deformed plagioclase feldspars. Physics and Chemistry of Mineral 11, 153–160.

Paterson, M.S., Weiss, L.E., 1961. Symmetry concepts in the structural analysis of deformed rocks. Bulletin of Geological Society of America 72, 841–882.

Prior, D.J., 1999. Problems in determining the orientations of crystal misorientation axes, for small angular misorientations, using electron backscatter diffraction in the SEM. Journal of Microscopy 195, 217–225.

Prior, J.D., Wheeler, J., 1999. Feldspar fabrics in a greeschist facies albite-rich mylonite from electron backscatter diffraction. Tectonophysics 303, 29–49.

Prior, D.J., Trimby, P.W., Weber, U.D., Dingley, D.J., 1996. Orientation

contrast imaging of microstructures in rocks using forescatter detectors in the scanning electron microscope. Mineralogical Magazine 60, 859–869.

Prior, D.J., Boyle, A., Brenker, F., Cheadal, M.C., Day, A., Lopez, G., Peruzzo, L., Potts, G.J., Reddy, S., Spiess, R., Timms, N.E., Trimby, P., Wheeler, J., Zetterstroem, L., 1999. The application of electron backscatter diffraction and orientation contrast imaging in the SEM to textural problem in rocks. American Mineralogist 84, 1741–1759.

Randle, V., 1992. Microtexture Determination and its Applications. The Institute of Materials, London.

Randle, V., 1993. The Measurement of Grain Boundary Geometry. Electron Microscopy in Materials Sciences Series, IOP, Bristol.

Reddy, S.M., Wheeler, J., Cliff, R.A., 1999. The geometry and timing of orogenic extension: an example from the western Italian Alps. Journal of Metamorphic Geology 17, 573–589.

Schmid, S.M., Casey, M., 1986. Complete fabric analysis of some commonly observed quartz *c*-axis patterns. In: Hobbs, B.E., Heard, H.C. (Eds.), Mineral and Rock Deformation: Laboratory Studies—The Paterson Volume, American Geophysical Union, Geophysical Monograph 36, pp. 263–286.

Smith, J.V., 1974. Feldspar Minerals, Volume 1: Crystal Structure and Physical Properties. Springer-Verlag, Berlin.

Stünitz, H., 1993. Transition from fracturing to viscous flow in a naturally deformed metagabbro. In: Boland, J.N., Fitz Gerald, J.F. (Eds.), Defects and Processes in the Solid State: Geosciences Applications. Elsevier, Amsterdam, pp. 121–150.

Trimby, P.W., 1998. Quantifying microstructures—the development and application of a new technique to quartzitic shear zones. Ph.D. thesis, University of Liverpool.

Trimby, P.W., Prior, J.D., Wheeler, J., 1998. Grain boundary hierarchy development in a quartz mylonite. Journal of Structural Geology 20, 917–935.

Venables, J.A., Harland, C.J., 1972. Electron back-scattering patterns—a new technique for obtaining crystallographic information in the scanning electron microscope. Philosophical Magazine 27, 1193–1200.

Wenk, H.-R., Christie, J.M., 1991. Comments on the interpretation of deformation textures in rocks. Journal of Structural Geology 13, 1091–1110.

Wenk, H.-R., Canova, G., Molinari, A., Kocks, U.F., 1989. Viscoplastic modelling of texture development in quartzite. Journal of Geophysical Research 94B, 17895–17906.

Wheeler, J., Butler, R.W.H., 1993. Evidence for extension in the Western Alpine orogen: the contact between the oceanic Piemonte and overlying Sesia Units. Earth and Planetary Sciences Letters 117, pp. 457–474.

Wheeler, J., Prior, D.J., Jiang, Z., Spiess, R., Trimby, P.W. (in review). The petrological significance of misorientations between grains.

Wilkinson, A.J., Hirsch, P.B., 1997. Electron diffraction based techinques in scanning electron microscopy of bulk materials. Journal of Microscopy 28, 279–308.